COMPUTER ANIMATION AND VIRTUAL WORLDS
Comp. Anim. Virtual Worlds 2009; **20**: 457–472
Published online 7 January 2009 in Wiley InterScience
(www.interscience.wiley.com) DOI: 10.1002/cav.274

Spatial camera orientation control by rotation-minimizing directed frames

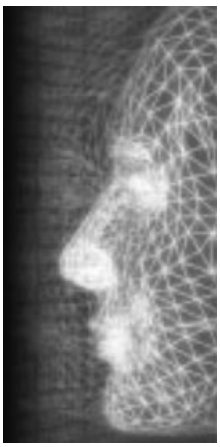

By Rida T. Farouki and Carlotta Giannelli*

The use of rotation-minimizing directed frames (RMDFs) for defining smoothly varying camera orientations along given spatial paths, in real or virtual environments, is proposed. A directed frame on a space curve $\mathbf{r}(\xi)$ ***is a varying orthonormal basis*** $(\mathbf{o}, \mathbf{p}, \mathbf{q})$ ***for*** $\mathbb{R}^3$ ***such that*** $\mathbf{o}(\xi) = \mathbf{r}(\xi)/|\mathbf{r}(\xi)|$ ***coincides with the unit polar vector from the origin to each curve point, and such a frame is rotation-minimizing if its angular velocity vector*** $\boldsymbol{\omega}$ ***maintains a vanishing component along*** $\mathbf{o}$***. To facilitate computation of rotation-minimizing directed frames, it is shown that the basic theory is equivalent to the established theory for rotation-minimizing adapted frames—for which one frame vector coincides with the tangent*** $\mathbf{t}(\xi) = \mathbf{r}'(\xi)/|\mathbf{r}'(\xi)|$ ***at each curve point—if one replaces the given space curve by its anti-hodograph (i.e., indefinite integral). A family of polynomial curves on which RMDFs can be computed exactly by a rational function integration, the Pythagorean (P) curves, is also introduced, together with algorithms for their construction. Copyright © 2009 John Wiley & Sons, Ltd.***

Received: 3 April 2008; Revised: 15 October 2008; Accepted: 27 October 2008

KEY WORDS: camera orientation; directed frames; angular velocity; rotation-minimizing frames; anti-hodograph; Pythagorean curves

Introduction

The motion of a rigid body in $\mathbb{R}^3$ can be described in terms of the trajectory of a distinguished point of the body (e.g., the center of mass) and the variation of an orthonormal frame, specifying the orientation of the body, along this trajectory. Such a description essentially decomposes the spatial motion into coordinated linear and angular velocity components.

Typically, the translational motion component is straightforward, and it is the orientational component that poses difficulty. A common circumstance is that the variation of the orientational frame is partially constrained, and one must then identify an "optimal" choice for specifying its residual degrees of freedom. The most commonly studied case concerns the so-called *adapted* frames on space curves, in which one frame vector is coincident with the curve tangent. This is a natural choice in, for example, specifying the motion of an aircraft or spacecraft, in which a principal axis of the vehicle remains aligned with its trajectory, or in constructing a *swept surface* through the motion of a planar "profile curve" along a "sweep curve," such that the plane containing the profile curve always remains orthogonal to the sweep curve.

An infinitude of adapted frames exists on any given space curve, due to the residual freedom associated with the orientation of the basis vectors that span the normal plane (orthogonal to the tangent vector) at each point. The most familiar adapted frame—the *Frenet frame*—is often a poor choice for motion planning or swept surface constructions, since it incurs "unnecessary" rotation of the basis vectors in the normal plane. The fact that the principal normal vector always points to the center of curvature often yields awkward-looking motions, or unreasonably "twisted" swept surfaces.

To address this problem, the construction of *rotation-minimizing* adapted frames on space curves has recently been the subject of intensive study. The advantages of rotation-minimizing frames for construction of swept surfaces were first noted by Klok,[1] who characterized them as solutions to certain differential equations. Guggenheimer[2] subsequently showed that solutions to these equations correspond to frame vectors in the normal plane with an angular orientation relative to the

*Correspondence to: Rida T. Farouki, Department of Mechanical and Aeronautical Engineering, University of California, Davis, CA 95616, U.S.A. E-mail: farouki@ucdavis.edu

principal normal and binormal specified (modulo a constant) by the integral of the curve torsion with respect to arc length. It was observed in Reference [3] that, for Pythagorean-hodograph (PH) curves, this angle function admits closed-form evaluation through rational function integration. The piecewise-rational approximation of rotation-minimizing adapted frames is described in References [4–8].

Rather than an *adapted* frame along a space curve, we consider here the notion of a *directed* frame along the curve. Whereas one vector of an adapted frame is determined by the curve tangent at each point, the direction from a fixed point in space (conventionally chosen as the origin) to each curve point determines one vector of a directed frame. As with the adapted frames, there exists an infinitude of directed frames compatible with this constraint, and it is again desirable to identify the *rotation-minimizing* directed frames (RMDFs). In fact, the theories of rotation-minimizing *adapted* frames and *directed* frames are intimately connected—the former theory carries over identically to the latter context, when applied to the *anti-hodograph* (indefinite integral) $\mathbf{s}(\xi)$ of the given space curve $\mathbf{r}(\xi)$, rather than the curve itself.

A key motivation for studying RMDFs arises from the problem of specifying camera motion relative to a fixed object. The problem pertains to both a real "physical" camera used in the production of a movie or in a video inspection process, and a "virtual" camera in a simulated environment, as in computer games or *virtual reality* software. It is presumed that a motion of the camera center along a space curve is prescribed, during which its optical axis must always point toward a stationary object located at the origin. This fixes the unit polar vector as one member of the orthonormal frame that specifies the camera orientation, but—as with adapted frames—a residual degree of freedom exists, associated with the basis vectors spanning the plane orthogonal to this polar vector (i.e., the camera *image plane*). The use of an RMDF to specify the orientation of the camera frame yields the least possible apparent image rotation within the frame, consistent with execution of the given spatial path. To achieve this, a physical camera mount must incorporate a third rotational freedom, about the camera optical axis, in addition to the usual altitude and azimuth axes. For a "virtual" camera, of course, the rotation-minimizing property can be achieved in software at minimal computational cost.

The structure of this paper is as follows. After discussing some potential applications, we briefly review the familiar theory of the Frenet adapted frame on a space curve, and show how *rotation-minimizing* adapted frames can be obtained from it. The idea of a *directed* frame on a space curve, relative to a fixed point, is introduced, and a special case—the Frenet directed frame—is identified by analogy with the Frenet adapted frame. The variation of the Frenet directed frame is then described in terms of the *polar curvature* and the *polar torsion*, analogs of the "ordinary" curvature and torsion governing the Frenet adapted frame. Properties of the *anti-hodograph* (indefinite integral) of a parametric space curve, a concept that elucidates relationships between the Frenet adapted and directed frames, are also analyzed. The computation of RMDFs is then addressed, arguing again by analogy with the theory of adapted frames. Finally, the possibility of exact computation of such frames by a rational function integration, for the special family of *Pythagorean curves*, is investigated.

Camera Image Orientation

Although the focus of this paper is on developing basic theory and algorithms for the computation of RMDFs on space curves, we briefly mention here some potential applications to motivate this problem. The problem of camera motion planning within real or virtual environments, already mentioned above, has been considered by numerous authors—for example References [9,10]. Such studies typically address global qualitative aspects of the camera path, and seek to formulate an automatic (or semi-automatic) means of generating a "natural" image perspective while avoiding collisions or obscurations of the camera by obstacles in the environment.

The precise specification of the image frame orientation about the camera "roll" axis, as it traverses a prescribed spatial path, does not appear to have received much attention. For a physical camera on a mount that offers three translational and two rotational (altitude and azimuth) degrees of freedom, the image frame orientation is completely determined by the requirement of maintaining a "target" object[†] centered in the field of view. Thus, a physical camera mount must offer a third rotational freedom, about the optical axis, to provide full control over the image frame orientation. Alternatively, for a digital camera with a circular field of view, this freedom can be emulated by software image rotations. For a *virtual* camera within a computer-modeled environment, complete control of image frame orientation is readily available using simple geometric image transformations.

[†]Conventionally, we take a target object fixed at the origin, although a moving target is easily accommodated by considering only the *relative* motion between camera and target.

DOI: 10.1002/cav

Hence, as the camera executes a complicated path, it is easy to implement the variation of the image frame orientation that ensures the "least possible" apparent rotation of the target object relative to the (typically rectangular) image frame boundary.

Besides cinematography, video games, and "virtual reality" applications, another possible application is in the medical practice of *endoscopic surgery*. This is a minimally invasive surgical procedure, in which the surgeon makes a small incision in the abdomen of a patient, through which a flexible tube is inserted. The end of this tube carries a miniature CCD camera and surgical instrument, which are guided to the target tissue while the surgeon monitors the procedure through a video display—the image is conveyed through the flexible tube by a coherent fiber optic bundle. Since the surgeon has a rather limited view of tissue at the current endoscope location and its environs, the process of guiding it to the target tissue and performing the surgery through this imperfect visual feedback can be quite difficult.[11–14]

A number of patents describing systems to automatically orient endoscope images relative to a "preferred" direction (typically, the force of gravity) have been issued—for example, see References [15,16]. Such methods employ accelerometers or other electronic sensors to continuously measure the current CCD camera orientation and apply compensating rotations to the displayed image. This helps minimize the likelihood of the surgeon being disoriented by unexpected or unnecessary rotation of the displayed image. If the endoscope must follow a curved path to reach the target tissue from the insertion point, while avoiding other organs, some image rotation (relative to the initial camera position) is inevitable. The RMDFs offer a mathematically rigorous identification of the variation of camera orientation that yields the least possible image rotation, allowing it to be cancelled through software transformations. This feature may be especially advantageous in the planning and execution of endoscope paths using abdomenal CAT scan data.

An analogous problem is addressed by a *field de-rotator* for a telescope on an altazimuth mount. When a telescope takes a long exposure of a celestial object, it must compensate for the apparent motion of the object on the sky caused by the earth's rotation. An equatorial telescope mount, in which one axis is parallel to the earth's axis of rotation, and rotates in the opposite sense at a rate of 1 revolution/day, has traditionally been employed to achieve this. In recent years, however, there has been greater emphasis on using "simple" altazimuth mounts with more sophisticated computer controls independently driving the altitude and azimuth axes, to achieve precision diurnal tracking. However, this incurs an apparent rotation of the telescope field of view, which must be cancelled out by the field de-rotator.

Other possible applications include orientational path planning for surface inspection probes with anisotropic sensors, and video inspections of aircraft engines, gas turbines, pipes, and other confined spaces. It is beyond the scope of this paper to dwell on the technical details of particular applications. Our focus is, instead, on developing the basic theory of RMDFs, and algorithms for their computation. It is known[4] that, if a space curve is modeled as an elastic fiber subject to bending and twisting, the least value of the elastic strain energy will be achieved when the "twist" angle is specified by a rotation-minimizing adapted frame. Analogously, the RMDFs identify solutions to a similar minimum-energy problem involving orientation relative to a fixed point in space, and thus deserve to be more systematically studied.

The Frenet Adapted Frame

The *parametric speed* of a space curve $\mathbf{r}(\xi) = (x(\xi), y(\xi), z(\xi))$ is the function

$$\sigma(\xi) = |\mathbf{r}'(\xi)| = \sqrt{x'^2(\xi) + y'^2(\xi) + z'^2(\xi)} \qquad (1)$$

of the curve parameter ξ, that defines the rate of change $\mathrm{d}s/\mathrm{d}\xi$ of the curve arc length s with ξ. We consider only curves that satisfy $\sigma(\xi) \neq 0$ for all ξ. Derivatives with respect to the arc length s and parameter ξ are related by

$$\frac{\mathrm{d}}{\mathrm{d}s} = \frac{1}{\sigma}\frac{\mathrm{d}}{\mathrm{d}\xi}$$

The type of orthonormal frame most often used for specifying orientation on a space curve is an *adapted* frame, in which the curve *tangent*

$$\mathbf{t}(\xi) = \frac{\mathbf{r}'(\xi)}{\sigma(\xi)} \qquad (2)$$

is specified as one of the three frame vectors, and the other two vectors span the *normal plane* at each point. A familiar adapted frame on a space curve is the *Frenet frame*, defined[17] by

$$\mathbf{t} = \frac{\mathbf{r}'}{|\mathbf{r}'|} \qquad \mathbf{n} = \frac{\mathbf{r}' \times \mathbf{r}''}{|\mathbf{r}' \times \mathbf{r}''|} \times \mathbf{t} \qquad \mathbf{b} = \frac{\mathbf{r}' \times \mathbf{r}''}{|\mathbf{r}' \times \mathbf{r}''|} \qquad (3)$$

DOI: 10.1002/cav

At each point, the principal normal $\mathbf{n}$ points toward the *center of curvature*, while the binormal $\mathbf{b} = \mathbf{t} \times \mathbf{n}$ complements $\mathbf{t}$ and $\mathbf{n}$ so that $(\mathbf{t}, \mathbf{n}, \mathbf{b})$ comprise a right-handed frame. The Frenet frame orientation is thus determined by the *intrinsic curve geometry*. The three mutually perpendicular planes spanned by the vector pairs $(\mathbf{n}, \mathbf{b})$, $(\mathbf{t}, \mathbf{n})$, and $(\mathbf{b}, \mathbf{t})$ at each point of a curve $\mathbf{r}(\xi)$ are known as the *normal*, *osculating*, and *rectifying* planes.

The normal plane is orthogonal to the curve tangent $\mathbf{t}$—it "cuts the curve orthogonally" at each point $\mathbf{r}(\xi)$. The osculating plane exhibits *second-order contact* with the curve—it is the plane that "most nearly contains the curve" in some neighborhood of each point. Finally, the set of rectifying planes to a space curve envelope a ruled surface, known as the *rectifying developable* of that curve. A developable surface, regarded as a thin material sheet, may be "flattened" onto a plane without stretching or compressing the material—the space curve embedded in the rectifying developable is "rectified" by this process into a *straight line* of exactly the same total length.

Henceforth we adopt the practice of calling vectors (3) the *Frenet adapted frame*, since we shall subsequently introduce an analogous type of frame called the *Frenet directed frame*. The variation of the frame vectors (3) on $\mathbf{r}(\xi)$ can be described in terms of the *curvature* and *torsion* functions, defined by

$$\kappa = \frac{|\mathbf{r}' \times \mathbf{r}''|}{|\mathbf{r}'|^3} \quad \text{and} \quad \tau = \frac{(\mathbf{r}' \times \mathbf{r}'') \cdot \mathbf{r}'''}{|\mathbf{r}' \times \mathbf{r}''|^2}$$

Namely, the derivatives of vectors (3) with respect to the curve arc length s are given[17] by the *Frenet–Serret equations*

$$\frac{\mathrm{d}\mathbf{t}}{\mathrm{d}s} = \kappa\mathbf{n} \quad \frac{\mathrm{d}\mathbf{n}}{\mathrm{d}s} = -\kappa\mathbf{t} + \tau\mathbf{b} \quad \frac{\mathrm{d}\mathbf{b}}{\mathrm{d}s} = -\tau\mathbf{n} \tag{4}$$

In terms of derivatives with respect to the curve parameter ξ, these equations can be expressed in matrix form as

$$\begin{bmatrix} \mathbf{t}' \\ \mathbf{n}' \\ \mathbf{b}' \end{bmatrix} = \sigma \begin{bmatrix} 0 & \kappa & 0 \\ -\kappa & 0 & \tau \\ 0 & -\tau & 0 \end{bmatrix} \begin{bmatrix} \mathbf{t} \\ \mathbf{n} \\ \mathbf{b} \end{bmatrix} \tag{5}$$

where the parametric speed $\sigma(\xi)$ is defined by Equation (1).

In order to describe the angular velocity[‡] of the frame $(\mathbf{t}, \mathbf{n}, \mathbf{b})$ as a whole, we introduce[17] the *Darboux vector*

$$\mathbf{d} = \kappa\mathbf{b} + \tau\mathbf{t} \tag{6}$$

in terms of which the relations (4) can be written as

$$\frac{\mathrm{d}\mathbf{t}}{\mathrm{d}s} = \mathbf{d} \times \mathbf{t} \quad \frac{\mathrm{d}\mathbf{n}}{\mathrm{d}s} = \mathbf{d} \times \mathbf{n} \quad \frac{\mathrm{d}\mathbf{b}}{\mathrm{d}s} = \mathbf{d} \times \mathbf{b} \tag{7}$$

Hence, the rate of change of the frame $(\mathbf{t}, \mathbf{n}, \mathbf{b})$ with s can be characterized as an instantaneous rotation about the vector $\mathbf{d}$, with angular speed equal to the *total curvature* specified by $\omega = |\mathbf{d}| = \sqrt{\kappa^2 + \tau^2}$.

It should be noted that, at points where $\kappa = 0$, the principal normal $\mathbf{n}$ and binormal $\mathbf{b}$ specified by Equation (3) are indeterminate. Such points are called the *inflections* of a space curve, and $\mathbf{n}$ and $\mathbf{b}$ ordinarily suffer sudden reversals upon traversing them. For a space curve with $\sigma(\xi) \neq 0$ for all ξ, the curvature can vanish only if (i) $\mathbf{r}''(\xi) = \mathbf{0}$, or (ii) $\mathbf{r}'(\xi)$ and $\mathbf{r}''(\xi)$ are parallel.

Rotation-minimizing Adapted Frames

The Darboux vector (6) gives the instantaneous angular velocity of the Frenet adapted frame on a space curve. From Equation (4) we observe that $\mathbf{t}$ changes at rate κ in the direction of $\mathbf{n}$. The change of $\mathbf{n}$ has two components: rate $-\kappa$ in the direction of $\mathbf{t}$, and rate τ in the direction of $\mathbf{b}$. Finally, $\mathbf{b}$ changes at rate $-\tau$ in the direction of $\mathbf{n}$. Now changes in the direction of $\mathbf{t}$ are inevitable if we require an adapted frame, that incorporates $\mathbf{t}$ as one basis vector. However, the change of $\mathbf{n}$ in the direction of $\mathbf{b}$, and of $\mathbf{b}$ in the direction of $\mathbf{n}$, correspond to a rotation of these vectors within the normal plane, a consequence of the fact that $\mathbf{n}$ always points toward the center of curvature.

As noted by Bishop[18] "there is more than one way to frame a curve," and a rotation-minimizing adapted frame $(\mathbf{e}_1, \mathbf{e}_2, \mathbf{e}_3)$ with $\mathbf{e}_1 = \mathbf{t}$ is characterized by the fact that its angular velocity vector $\boldsymbol{\omega}$ omits the component $\tau\mathbf{t}$ from the Darboux vector (6) and is thus simply $\boldsymbol{\omega} = \kappa\mathbf{b}$. The basis vectors $(\mathbf{e}_2, \mathbf{e}_3)$ can be obtained from $(\mathbf{n}, \mathbf{b})$ by

[‡]In speaking of the *angular velocity* of a frame along a space curve, we imagine the curve to be traversed at unit speed, so the arc length s and elapsed time t are equivalent.

DOI: 10.1002/cav

a rotation

$$\begin{bmatrix} \mathbf{e}_2 \\ \mathbf{e}_3 \end{bmatrix} = \begin{bmatrix} \cos\psi & \sin\psi \\ -\sin\psi & \cos\psi \end{bmatrix} \begin{bmatrix} \mathbf{n} \\ \mathbf{b} \end{bmatrix} \tag{8}$$

in the normal plane, specified by an appropriate angle function $\psi(\xi)$.

Klok[1] showed that the basis vectors ($\mathbf{e}_2$, $\mathbf{e}_3$) of a rotation-minimizing adapted frame must satisfy the differential equations

$$\mathbf{e}_k'(\xi) = -\frac{\mathbf{r}''(\xi)\cdot\mathbf{e}_k(\xi)}{|\mathbf{r}'(\xi)|^2}\mathbf{r}'(\xi), \quad k = 2, 3$$

Substituting from Equation (8), one can verify that these amount to the equation

$$\frac{\mathrm{d}\psi}{\mathrm{d}\xi} = -|\mathbf{r}'|\tau = -|\mathbf{r}'|\frac{(\mathbf{r}'\times\mathbf{r}'')\cdot\mathbf{r}'''}{|\mathbf{r}'\times\mathbf{r}''|^2} \tag{9}$$

for the rotation angle $\psi(\xi)$ used to obtain ($\mathbf{e}_2$, $\mathbf{e}_3$) from ($\mathbf{n}$, $\mathbf{b}$) in Equation (8). Hence, as observed by Guggenheimer,[2] this function has the form[§]

$$\psi(\xi) = \psi_0 - \int_0^{\xi} \tau(u)\sigma(u)\,\mathrm{d}u \tag{10}$$

The above integral does not admit analytic reduction for the commonly used polynomial and rational curves. Hence, several schemes have been proposed to approximate rotation minimizing adapted frames on a given curve, or to approximate a given curve by "simpler" segments (e.g., circular arcs) with known rotation-minimizing frames.[5–8] The spatial PH curves are an exception[3]—for these curves the integrand reduces to a rational function, which may be integrated by first computing its partial fraction decomposition.

The Frenet Directed Frame

For a space curve $\mathbf{r}(\xi) = (x(\xi), y(\xi), z(\xi))$ the function

$$\rho(\xi) = |\mathbf{r}(\xi)| = \sqrt{x^2(\xi) + y^2(\xi) + z^2(\xi)} \tag{11}$$

specifies the radial distance of each curve point from the origin. If $\rho(\xi) \neq 0$ for all ξ, we can define a unit *polar vector* at each curve point by

$$\mathbf{o}(\xi) = \frac{\mathbf{r}(\xi)}{\rho(\xi)} \tag{12}$$

Since the polar vector is always specified by the direction from the origin to each curve point, we call an orthonormal frame that incorporates this vector as one component a *directed* frame on the curve.

If the curve satisfies $\sigma(\xi) \neq 0$ for all ξ, and the tangent (2) is thus defined at each point, we can employ $\mathbf{o}(\xi)$ and $\mathbf{t}(\xi)$ to define a "canonical" directed frame, in a manner analogous to that of the Frenet adapted frame (3). Upon replacing $\mathbf{r}'$, $\mathbf{r}''$, $\mathbf{r}'''$ in Equation (3) by $\mathbf{r}$, $\mathbf{r}'$, $\mathbf{r}''$ we obtain the directed frame defined by

$$\mathbf{o} = \frac{\mathbf{r}}{|\mathbf{r}|} \quad \mathbf{u} = \frac{\mathbf{r}\times\mathbf{r}'}{|\mathbf{r}\times\mathbf{r}'|}\times\mathbf{o} \quad \mathbf{v} = \frac{\mathbf{r}\times\mathbf{r}'}{|\mathbf{r}\times\mathbf{r}'|} \tag{13}$$

Because of its close relation to Equation (3), we call this "canonical" directed frame the *Frenet directed frame*. The definition of the frame ($\mathbf{o}$, $\mathbf{u}$, $\mathbf{v}$) motivates us to introduce the *anti-hodograph*[‖] of a space curve $\mathbf{r}(\xi)$. Just as the hodograph is the derivative $\mathbf{r}'(\xi)$, regarded as a parametric curve in its own right, the anti-hodograph is the indefinite integral $\int \mathbf{r}(\xi)\,\mathrm{d}\xi$—also viewed as a parametric curve (there are infinitely many anti-hodographs, because of the arbitrary integration constant, but they are merely translates of each other).

Comparing Equation (3) with Equation (13), we see that the Frenet directed frame is simply *the Frenet adapted frame of the anti-hodograph* of $\mathbf{r}(\xi)$. This means that we can write the derivative of the frame (13) in a form analogous to Equation (5) as

$$\begin{bmatrix} \mathbf{o}' \\ \mathbf{u}' \\ \mathbf{v}' \end{bmatrix} = \rho \begin{bmatrix} 0 & \lambda & 0 \\ -\lambda & 0 & \upsilon \\ 0 & -\upsilon & 0 \end{bmatrix} \begin{bmatrix} \mathbf{o} \\ \mathbf{u} \\ \mathbf{v} \end{bmatrix} \tag{14}$$

where the functions

$$\rho = |\mathbf{r}| \quad \lambda = \frac{|\mathbf{r}\times\mathbf{r}'|}{|\mathbf{r}|^3} \quad \upsilon = \frac{(\mathbf{r}\times\mathbf{r}')\cdot\mathbf{r}''}{|\mathbf{r}\times\mathbf{r}'|^2} \tag{15}$$

define the parametric speed, curvature, and torsion of the anti-hodograph.

As previously noted, the polar vector $\mathbf{o}(\xi)$ specifies the direction from the origin to each point of the curve $\mathbf{r}(\xi)$.

[§] An incorrect sign before the integral is given in Reference [2].

[‖] We choose this term by analogy with the occasional usage of *anti-derivative* to denote the indefinite integral of a function.

DOI: 10.1002/cav

Frenet adapted frame	Frenet directed frame
Tangent vector $\mathbf{t}$	Polar vector $\mathbf{o}$
Principal normal $\mathbf{n}$	Principal axis $\mathbf{u}$
Binormal vector $\mathbf{b}$	Bi-axis vector $\mathbf{v}$
Normal plane = span($\mathbf{n}$, $\mathbf{b}$)	Image plane = span($\mathbf{u}$, $\mathbf{v}$)
Osculating plane = span($\mathbf{t}$, $\mathbf{n}$)	Motion plane = span($\mathbf{o}$, $\mathbf{u}$)
Rectifying plane = span($\mathbf{b}$, $\mathbf{t}$)	Orthogonal plane = span($\mathbf{v}$, $\mathbf{o}$)
Parametric speed σ	Polar distance ρ
Curvature κ	Polar curvature λ
Torsion τ	Polar torsion υ

Table 1. Corresponding properties of Frenet *adapted* and *directed* frames

In the context of a camera that moves along $\mathbf{r}(\xi)$ and is always aimed toward an object located at the origin, $\mathbf{o}(\xi)$ defines the *optical axis* of the camera lens. Thus, the plane orthogonal to the vector $\mathbf{o}$—spanned by the vectors ($\mathbf{u}$, $\mathbf{v}$)—is called the *image plane*.

At each point of $\mathbf{r}(\xi)$, the orthogonal unit vectors ($\mathbf{u}$, $\mathbf{v}$) may be regarded as specifying Cartesian axes in the image plane. By analogy with the Frenet adapted frame, we call $\mathbf{u}$ the *principal axis* and $\mathbf{v}$ the *bi-axis* for the image plane. These axes vary as the camera traverses the path $\mathbf{r}(\xi)$ while pointing toward the origin—their variation is described by Equation (14).

We have called the plane through each curve point $\mathbf{r}(\xi)$ that is orthogonal to $\mathbf{o}$—i.e., spanned by ($\mathbf{u}$, $\mathbf{v}$)—the image plane. Consider now the plane orthogonal to $\mathbf{v}$ at each curve point, spanned by ($\mathbf{o}$, $\mathbf{u}$). We observe from Equation (13) that $\mathbf{v}$ is perpendicular to $\mathbf{t}$, so this plane must be *tangent* to the curve at the point $\mathbf{r}(\xi)$. Since the instantaneous camera trajectory lies in this plane, we call it the *motion plane*. Finally, the plane that is orthogonal to $\mathbf{u}$ at each point of $\mathbf{r}(\xi)$—spanned by ($\mathbf{v}$, $\mathbf{o}$)—is mutually perpendicular to the image and motion planes: we call it the *orthogonal* plane.

Table 1 enumerates the correspondence of geometrical entities associated with the Frenet adapted and directed frames. We have also introduced here the terms *polar curvature* and *polar torsion* as synonyms for the curvature λ and torsion υ of the anti-hodograph[¶]—as defined by Equation (15).

A *regular* space curve is characterized by the property that its first and second derivatives, $\mathbf{r}'(\xi)$ and $\mathbf{r}''(\xi)$, are linearly independent for all ξ (which implies that they are non-vanishing for all ξ). For a regular curve, the Frenet adapted frame ($\mathbf{t}$, $\mathbf{n}$, $\mathbf{b}$) is well defined at every point. By analogy with this notion of regularity, we define the concept of *polar regularity* as follows.

Definition 1. *A space curve $\mathbf{r}(\xi)$ is polar-regular if its anti-hodograph $\mathbf{s}(\xi)$ is regular, that is, $\mathbf{r}(\xi)$ and $\mathbf{r}'(\xi)$ are always linearly independent. Polar-regular curves have well-defined Frenet directed frames at each point, given by Equation (13).*

Since the Frenet adapted and directed frames are both orthonormal bases for $\mathbb{R}^3$ at each curve point, it is possible to express one in terms of the other. The relationship is given by

$$\begin{bmatrix} \mathbf{o} \\ \mathbf{u} \\ \mathbf{v} \end{bmatrix} = \begin{bmatrix} \mathbf{o}\cdot\mathbf{t} & \mathbf{o}\cdot\mathbf{n} & \mathbf{o}\cdot\mathbf{b} \\ \mathbf{u}\cdot\mathbf{t} & \mathbf{u}\cdot\mathbf{n} & \mathbf{u}\cdot\mathbf{b} \\ \mathbf{v}\cdot\mathbf{t} & \mathbf{v}\cdot\mathbf{n} & \mathbf{v}\cdot\mathbf{b} \end{bmatrix} \begin{bmatrix} \mathbf{t} \\ \mathbf{n} \\ \mathbf{b} \end{bmatrix}$$

where, using basic vector identities, the matrix elements may be written as

$$\mathbf{o}\cdot\mathbf{t} = \frac{\mathbf{r}\cdot\mathbf{r}'}{\rho\sigma}$$

$$\mathbf{o}\cdot\mathbf{n} = -\frac{(\mathbf{r}\times\mathbf{r}')\cdot(\mathbf{r}'\times\mathbf{r}'')}{\rho\sigma|\mathbf{r}'\times\mathbf{r}''|}$$

$$\mathbf{o}\cdot\mathbf{b} = \frac{(\mathbf{r}\times\mathbf{r}')\cdot\mathbf{r}''}{\rho|\mathbf{r}'\times\mathbf{r}''|}$$

$$\mathbf{u}\cdot\mathbf{t} = \frac{|\mathbf{r}\times\mathbf{r}'|}{\rho\sigma}$$

$$\mathbf{u}\cdot\mathbf{n} = \frac{\mathbf{r}\cdot\mathbf{r}'}{\rho\sigma}\,\frac{(\mathbf{r}\times\mathbf{r}')\cdot(\mathbf{r}'\times\mathbf{r}'')}{|\mathbf{r}\times\mathbf{r}'|\,|\mathbf{r}'\times\mathbf{r}''|}$$

$$\mathbf{u}\cdot\mathbf{b} = -\frac{(\mathbf{r}\cdot\mathbf{r}')(\mathbf{r}\times\mathbf{r}')\cdot\mathbf{r}''}{\rho|\mathbf{r}\times\mathbf{r}'|\,|\mathbf{r}'\times\mathbf{r}''|}$$

$$\mathbf{v}\cdot\mathbf{t} = 0$$

[¶]The symbol υ adopted for polar torsion is the Greek letter "upsilon"—the character following τ in the alphabet—not the Roman v, which looks very similar.

DOI: 10.1002/cav

$$\mathbf{v}\cdot\mathbf{n} = \frac{\sigma(\mathbf{r}\times\mathbf{r}')\cdot\mathbf{r}''}{|\mathbf{r}\times\mathbf{r}'|\,|\mathbf{r}'\times\mathbf{r}''|}$$

$$\mathbf{v}\cdot\mathbf{b} = \frac{(\mathbf{r}\times\mathbf{r}')\cdot(\mathbf{r}'\times\mathbf{r}'')}{|\mathbf{r}\times\mathbf{r}'|\,|\mathbf{r}'\times\mathbf{r}''|}$$

These define an *orthogonal* matrix, corresponding to a member of the spatial rotation group SO(3). Hence, the inverse matrix that gives $(\mathbf{t}, \mathbf{n}, \mathbf{b})$ in terms of $(\mathbf{o}, \mathbf{u}, \mathbf{v})$ is the *transpose* of the above matrix. Another description of the map $(\mathbf{t}, \mathbf{n}, \mathbf{b}) \to (\mathbf{o}, \mathbf{u}, \mathbf{v})$ can be expressed[19] in terms of a unit quaternion $\mathcal{U} = \cos\frac{1}{2}\phi + \sin\frac{1}{2}\phi\ \mathbf{a}$, the unit vector $\mathbf{a}$ specifying the axis and the parameter ϕ the angle of a spatial rotation that maps the former frame onto the latter.

By analogy with the Darboux vector (6) the angular velocity of the Frenet direct frame $(\mathbf{o}, \mathbf{u}, \mathbf{v})$ can be expressed as

$$\mathbf{e} = \frac{\rho}{\sigma}(\lambda\mathbf{v} + \upsilon\mathbf{o}) \tag{16}$$

where the factor ρ/σ arises because the angular velocity of any unit vector is defined to be its derivative with respect to arc length s along the curve. In terms of this *polar Darboux vector* $\mathbf{e}$, we have

$$\frac{\mathrm{d}\mathbf{o}}{\mathrm{d}s} = \mathbf{e}\times\mathbf{o} \quad \frac{\mathrm{d}\mathbf{u}}{\mathrm{d}s} = \mathbf{e}\times\mathbf{u} \quad \frac{\mathrm{d}\mathbf{v}}{\mathrm{d}s} = \mathbf{e}\times\mathbf{v}$$

For the Frenet directed frame $(\mathbf{o}, \mathbf{u}, \mathbf{v})$ the magnitude of the angular velocity (16) is $|\mathbf{e}| = |\rho/\sigma|\sqrt{\lambda^2+\upsilon^2}$.

Polar Curvature and Torsion

The geometrical significance of the polar curvature and polar torsion may be characterized as follows.

Lemma 1. *When the polar curvature of a space curve* $\mathbf{r}(\xi)$ *satisfies* $\lambda(\xi) \equiv 0$, *the curve must be a straight line through the origin. Similarly, when the polar torsion satisfies* $\upsilon(\xi) \equiv 0$, *the curve resides in a plane through the origin.*

Proof. The polar curvature λ defined by Equation (15) vanishes identically if and only if $\mathbf{r}(\xi)$ and $\mathbf{r}'(\xi)$ are linearly dependent for all ξ, and this is the characteristic property of straight lines passing through the origin. Also, if the polar torsion υ specified by Equation (15) vanishes identically, the bi-axis vector $\mathbf{v}$ must be constant by Equation (14). Since $(\mathbf{o}, \mathbf{u}, \mathbf{v})$ comprise an orthonormal frame, we have $\mathbf{v}\cdot\mathbf{o} = 0$, and hence $\mathbf{v}\cdot\mathbf{r}(\xi) = 0$ from Equation (13). For constant $\mathbf{v}$, this characterizes $\mathbf{r}(\xi)$ as lying in the plane through the origin with normal vector $\mathbf{v}$. ■

Clearly, when the polar curvature $\lambda(\xi)$ vanishes identically, the "ordinary" curvature $\kappa(\xi)$ must also vanish identically, and likewise concerning the polar torsion $\upsilon(\xi)$ and the "ordinary" torsion $\tau(\xi)$. We may verify this directly as follows. If $\mathbf{r}(\xi)\times\mathbf{r}'(\xi) \equiv 0$, then $\mathbf{r}(\xi)$ and $\mathbf{r}'(\xi)$ must be parallel for all ξ. By differentiating, we obtain $\mathbf{r}(\xi)\times\mathbf{r}''(\xi) \equiv 0$, which implies that $\mathbf{r}(\xi)$ and $\mathbf{r}''(\xi)$ must also be parallel for all ξ. Hence, $\mathbf{r}'(\xi)$ and $\mathbf{r}''(\xi)$ are always parallel, and we have $\mathbf{r}'(\xi)\times\mathbf{r}''(\xi) \equiv 0$. We conclude that $\lambda \equiv 0 \Rightarrow \kappa \equiv 0$.

Concerning the torsion, if $[\mathbf{r}(\xi)\times\mathbf{r}'(\xi)]\cdot\mathbf{r}''(\xi) \equiv 0$ we must have $\mathbf{r}''(\xi) = \alpha(\xi)\mathbf{r}(\xi) + \beta(\xi)\mathbf{r}'(\xi)$ for suitable scalar functions $\alpha(\xi)$, $\beta(\xi)$. Differentiating the identity gives $[\mathbf{r}(\xi)\times\mathbf{r}'(\xi)]\cdot\mathbf{r}'''(\xi) \equiv 0$, so $\mathbf{r}'''(\xi) = \gamma(\xi)\mathbf{r}(\xi) + \delta(\xi)\mathbf{r}'(\xi)$ for suitable $\gamma(\xi)$, $\delta(\xi)$. Substituting for $\mathbf{r}''(\xi)$ and $\mathbf{r}'''(\xi)$, one can easily verify that $[\mathbf{r}'(\xi)\times\mathbf{r}''(\xi)]\cdot\mathbf{r}'''(\xi)$ vanishes identically. Hence, $\upsilon \equiv 0 \Rightarrow \tau \equiv 0$.

Instead of vanishing identically, the polar curvature and torsion may also vanish at discrete points of nondegenerate space curves. At such points, the Frenet directed frame (13) may exhibit singular behavior.

Definition 2. *A polar inflection of the space curve* $\mathbf{r}(\xi)$ *is a point where the polar curvature* $\lambda(\xi)$ *vanishes. The components* $(\mathbf{u}, \mathbf{v})$ *of the Frenet directed frame are indeterminate at such points.*

Polar inflections correspond to points where $\mathbf{r}(\xi)$ and $\mathbf{r}'(\xi)$ become linearly dependent. For polar-regular curves, this corresponds to situations in which the polar and tangent vectors satisfy $\mathbf{t} = \pm\mathbf{o}$. For curves that are not polar-regular, points where either $\mathbf{r}(\xi) = \mathbf{0}$ (traversals of the origin) or $\mathbf{r}'(\xi) = \mathbf{0}$ (stationary points) are also counted among the polar inflections.

Every point of a straight line through the origin is a polar inflection: the polar vector $\mathbf{o}$ is constant, but the other vectors $\mathbf{u}$, $\mathbf{v}$ of the Frenet directed frame are everywhere indeterminate. For a curve residing in a plane through the origin, the bi-axis vector $\mathbf{v}$ is constant (the normal to that plane), while the other vectors $\mathbf{o}$, $\mathbf{u}$ always lie in the plane. For straight lines that do not pass through the origin, and planar curves residing in planes that do not go through the origin, the Frenet directed frame $(\mathbf{o}, \mathbf{u}, \mathbf{v})$ and polar curvature and torsion λ and υ have no special distinctive behavior.

Remark 1. *A helical curve is characterized*[17,20–22] *by the fact that its tangent vector maintains a constant angle* ψ *with respect to a fixed direction defined by a unit vector* $\mathbf{a}$, *that*

DOI: 10.1002/cav

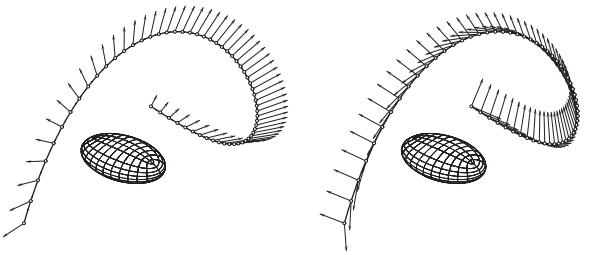

Figure 1. An ellipsoid is to be inspected by a camera that traverses a spatial path, keeping its optical axis passing through the center of the ellipsoid. Left: a sampling of the polar vectors $\mathbf{o}$ *along the path, specifying the orientation of the camera optical axis. Right: a sampling of the principal axis and bi-axis vectors of the Frenet directed frame,* $\mathbf{u}$ *and* $\mathbf{v}$*, that span the image plane.*

is, $\mathbf{a} \cdot \mathbf{t} = \cos\psi$*. Alternatively, its curvature and torsion exhibit the constant ratio* $\kappa/\tau = \tan\psi$*. Analogously, a polar helix is characterized by the fact that its polar vector satisfies* $\mathbf{a} \cdot \mathbf{o} = \cos\psi$ *for some fixed unit vector* $\mathbf{a}$ *and angle* ψ*, or by a constant ratio* $\lambda/\upsilon = \tan\psi$ *of polar curvature and torsion.*[**] *Such a curve must lie on a circular cone with apex at the origin,* $\mathbf{a}$ *and* ψ *being the cone axis and half-angle.*

Figure 1 shows the variation of the Frenet directed frame ($\mathbf{o}$, $\mathbf{u}$, $\mathbf{v}$) along a quintic Bézier curve. When this frame is used to orient a camera viewing an ellipsoid centered at the origin, the polar vector $\mathbf{o}$ specifies the optical axis, while the principal axis and bi-axis vectors $\mathbf{u}$ and $\mathbf{v}$ specify the orientation of the image frame in the image plane orthogonal to the optical axis.

Properties of the Anti-hodograph

Because of its importance in the theory of directed frames, and the apparent lack of prior discussion in the literature, we review here some basic properties of the anti-hodograph of a space curve $\mathbf{r}(\xi)$. For a degree n Bézier curve with control points $\mathbf{p}_0, \ldots, \mathbf{p}_n$

$$\mathbf{r}(\xi) = \sum_{k=0}^{n} \mathbf{p}_k \binom{n}{k} (1-\xi)^{n-k} \xi^k \tag{17}$$

the hodograph (derivative) curve

$$\mathbf{d}(\xi) = \mathbf{r}'(\xi) = \sum_{k=0}^{n-1} \mathbf{d}_k \binom{n-1}{k} (1-\xi)^{n-1-k} \xi^k$$

is defined by the n control points $\mathbf{d}_k = n(\mathbf{p}_{k+1} - \mathbf{p}_k)$ for $k = 0, \ldots, n-1$, while the anti-hodograph (indefinite integral) curve

$$\mathbf{s}(\xi) = \int \mathbf{r}(\xi)\, \mathrm{d}\xi = \sum_{k=0}^{n+1} \mathbf{s}_k \binom{n+1}{k} (1-\xi)^{n+1-k} \xi^k$$

has (modulo a vector integration constant) the $n+2$ control points

$$\mathbf{s}_k = \frac{1}{n+1} \sum_{j=0}^{k-1} \mathbf{p}_j \quad k = 0, \ldots, n+1$$

As is well-known, if the hodograph $\mathbf{d}(\xi)$ passes through the origin for $\xi = \xi_*$, the point $\mathbf{r}(\xi_*)$ is generally a *cusp* of the curve, since the tangent $\mathbf{t}$ generally suffers an abrupt reversal at $\xi = \xi_*$. Likewise, if a tangent line to $\mathbf{d}(\xi)$ passes through the origin for $\xi = \xi_*$, the point $\mathbf{r}(\xi_*)$ is generally an *inflection* of the curve, since the vectors $\mathbf{r}'(\xi_*)$ and $\mathbf{r}''(\xi_*)$ are parallel.

Since any curve $\mathbf{r}(\xi)$ is the hodograph of its anti-hodograph $\mathbf{s}(\xi)$, similar relations between these curves can be deduced. Namely, when the curve $\mathbf{r}(\xi)$ passes through the origin for $\xi = \xi_*$, the point $\mathbf{s}(\xi_*)$ is generally a *cusp* on the anti-hodograph. Likewise, if a tangent line to $\mathbf{r}(\xi)$ passes through the origin for $\xi = \xi_*$, the point $\mathbf{s}(\xi_*)$ is generally an *inflection* of the anti-hodograph. As previously noted, the curvature and torsion of the anti-hodograph $\mathbf{s}(\xi)$ are the *polar curvature* and *polar torsion* of the curve $\mathbf{r}(\xi)$.

Remark 2. *Clearly, any polynomial curve has a polynomial anti-hodograph, and conversely any polynomial anti-hodograph specifies (modulo translation) a unique polynomial curve. However, this correspondence does not extend to the anti-hodographs of rational curves, since rational functions may not have rational indefinite integrals—the anti-hodograph of a rational Bézier curve, for example, may incur transcendental (logarithm or arc-tangent) terms.*

[**] Equivalently, a polar helix is a curve whose anti-hodograph is an "ordinary" helix.

DOI: 10.1002/cav

Rotation-minimizing Directed Frames

Since $\rho = \sqrt{\mathbf{r}\cdot\mathbf{r}}$, the arc length derivative of the polar vector (12) is

$$\frac{\mathrm{d}\mathbf{o}}{\mathrm{d}s} = \frac{1}{\sigma}\frac{\mathrm{d}}{\mathrm{d}\xi}\frac{\mathbf{r}}{\rho} = \frac{\rho^2\mathbf{r}' - (\mathbf{r}\cdot\mathbf{r}')\mathbf{r}}{\sigma\rho^3} = \frac{(\mathbf{o}\times\mathbf{t})\times\mathbf{o}}{\rho}$$

which can be written as

$$\frac{\mathrm{d}\mathbf{o}}{\mathrm{d}s} = \boldsymbol{\omega}\times\mathbf{o} \qquad \text{with} \quad \boldsymbol{\omega} = \alpha\mathbf{o} + \frac{\mathbf{o}\times\mathbf{t}}{\rho} \tag{18}$$

where α is an arbitrary scalar function. If the curve $\mathbf{r}(\xi)$ is traversed at unit speed, $\boldsymbol{\omega}$ defines the *angular velocity* of the unit vector $\mathbf{o}$—arising from the requirement that it always points from the origin toward $\mathbf{r}(\xi)$.

As far as $\mathbf{o}$ is concerned, the component $\alpha\mathbf{o}$ of $\boldsymbol{\omega}$ is immaterial, since it specifies an instantaneous rotation of $\mathbf{o}$ about itself. However, if we consider $\mathbf{o}$ as a component of a *directed frame* $(\mathbf{o}, \mathbf{p}, \mathbf{q})$ with the instantaneous angular velocity $\boldsymbol{\omega}$, the component $\alpha\mathbf{o}$ is significant—it specifies the angular velocity of the frame vectors $(\mathbf{u}, \mathbf{v})$ spanning the plane orthogonal to $\mathbf{o}$.

By analogy with the *adapted* rotation-minimizing frames $(\mathbf{t}, \mathbf{e}_1, \mathbf{e}_2)$ on a space curve $\mathbf{r}(\xi)$—characterized by the fact that the frame vectors $(\mathbf{e}_1, \mathbf{e}_2)$ have zero angular velocity component in the direction of the tangent $\mathbf{t}$—a *directed* rotation-minimizing frame $(\mathbf{o}, \mathbf{p}, \mathbf{q})$ is defined by the property that the frame vectors $(\mathbf{p}, \mathbf{q})$ maintain a zero angular velocity component in the direction of the polar vector $\mathbf{o}$. Hence, setting $\alpha \equiv 0$ in Equation (18) so that

$$\boldsymbol{\omega} = \frac{\mathbf{o}\times\mathbf{t}}{\rho} = \frac{\mathbf{r}\times\mathbf{r}'}{\sigma\rho^2} = \frac{\rho}{\sigma}\lambda\mathbf{v} \tag{19}$$

an RMDF $(\mathbf{o}, \mathbf{p}, \mathbf{q})$ is specified in terms of this angular velocity function by the differential relations

$$\frac{\mathrm{d}\mathbf{o}}{\mathrm{d}s} = \boldsymbol{\omega}\times\mathbf{o} \quad \frac{\mathrm{d}\mathbf{p}}{\mathrm{d}s} = \boldsymbol{\omega}\times\mathbf{p} \quad \frac{\mathrm{d}\mathbf{q}}{\mathrm{d}s} = \boldsymbol{\omega}\times\mathbf{q} \tag{20}$$

Hence, the RMDFs corresponds to omitting the component $(\rho/\sigma)\upsilon\mathbf{o}$ from the Frenet directed frame angular velocity (16)—for the rotation-minimizing frame we have $|\boldsymbol{\omega}| = (\rho/\sigma)|\lambda|$, which can also be written as $|\sin\zeta|/\rho$ where ζ is the angle between the polar and hodograph vectors, $\mathbf{r}(\xi)$ and $\mathbf{r}'(\xi)$. Hence, $|\boldsymbol{\omega}|$ vanishes if $\mathbf{r}(\xi)$ and $\mathbf{r}'(\xi)$ are collinear—that is, the camera is moving directly toward or away from the origin. For a fixed relative orientation ζ of $\mathbf{r}(\xi)$ and $\mathbf{r}'(\xi)$, note that $|\boldsymbol{\omega}|$ is inversely proportional to the camera distance $\rho(\xi) = |\mathbf{r}(\xi)|$ from the origin.

To integrate Equations (20), an initial frame $(\mathbf{o}_0, \mathbf{p}_0, \mathbf{q}_0)$ for $s = \xi = 0$ must be specified. Now $\mathbf{o}_0 = \mathbf{r}(0)/\rho(0)$ is uniquely determined, but there is a one-parameter family of vector pairs $(\mathbf{p}_0, \mathbf{q}_0)$ consistent with the requirement that $(\mathbf{o}_0, \mathbf{p}_0, \mathbf{q}_0)$ must be a right-handed orthonormal frame. Hence, as with the adapted rotation-minimizing frames, there exists a one-parameter family of directed rotation-minimizing frames on a given space curve. Any two such frames exhibit a constant angular displacement between their $(\mathbf{p}, \mathbf{q})$ vectors along the curve. For brevity, the acronyms RMAF and RMDF will henceforth be used for rotation-minimizing adapted and directed frames.

Now since $\mathbf{o}$ is uniquely specified by Equation (12) and we can define $\mathbf{q}$ as $\mathbf{o}\times\mathbf{p}$, it suffices to determine $\mathbf{p}$. Invoking the angular velocity (19), converting back to derivatives with respect to ξ, and setting

$$k_x = \frac{yz' - y'z}{x^2+y^2+z^2} \quad k_y = \frac{zx' - z'x}{x^2+y^2+z^2} \quad k_z = \frac{xy' - x'y}{x^2+y^2+z^2}$$

we obtain from Equation (20) the linear system of first-order differential equations

$$\begin{bmatrix} p_x' \\ p_y' \\ p_z' \end{bmatrix} = \begin{bmatrix} 0 & -k_z & k_y \\ k_z & 0 & -k_x \\ -k_y & k_x & 0 \end{bmatrix} \begin{bmatrix} p_x \\ p_y \\ p_z \end{bmatrix}$$

(with non-constant coefficients) for the components (p_x, p_y, p_z) of $\mathbf{p}$. We note that the matrix elements are *rational functions* of the curve parameter ξ. A single first-order differential equation with non-constant coefficients may sometimes be integrated by identifying an appropriate integrating factor, but this approach does not, in general, extended to first-order systems.

Instead of attempting to construct RMDFs by direct integration of these equations, we argue by analogy with the construction of RMAFs. Namely, we express the RMDF basis vectors $(\mathbf{p}, \mathbf{q})$ that span the image plane in terms of the two Frenet directed frame vectors $(\mathbf{u}, \mathbf{v})$ given by Equation (13) in the form

$$\begin{bmatrix} \mathbf{p} \\ \mathbf{q} \end{bmatrix} = \begin{bmatrix} \cos\psi & \sin\psi \\ -\sin\psi & \cos\psi \end{bmatrix} \begin{bmatrix} \mathbf{u} \\ \mathbf{v} \end{bmatrix} \tag{21}$$

that is, $(\mathbf{p}, \mathbf{q})$ are obtained from $(\mathbf{u}, \mathbf{v})$ at each curve point by rotation through a suitable angle ψ in the plane orthogonal to $\mathbf{o}$. The advantage of this approach is that it reduces the RMDF computation to determining the scalar function $\psi(\xi)$ that relates $(\mathbf{p}, \mathbf{q})$ to the known vectors $(\mathbf{u}, \mathbf{v})$.

DOI: 10.1002/cav

Since, on replacing a curve by its anti-hodograph, the theory of RMDFs coincides with that of RMAFs, we deduce that the desired angle function in Equation (21) is given by

$$\psi(\xi) = \psi_0 - \int_0^\xi \upsilon(u)\rho(u)\,\mathrm{d}u \tag{22}$$

Comparing the integrals in Equations (10) and (22) we note that, for general polynomial or rational curves, the torsion $\tau(\xi)$ and $\upsilon(\xi)$ of a curve and its anti-hodograph are both rational in the parameter ξ, but since the corresponding parametric speeds $\sigma(\xi)$ and $\rho(\xi)$ specified by Equations (1) and (11) are *square roots* of polynomials, we cannot, in general, obtain a closed-form reduction of these integrals.

For the PH curves, σ is a polynomial in ξ, so the integrand in Equation (10) is a rational function,[3] and Equation (10) can be determined analytically by partial fraction decomposition. By analogy, we shall introduce below the Pythagorean (P) curves, for which ρ is a polynomial in ξ and the integrand in Equation (22) is thus rational, allowing exact RMDF computation.

Example 1. Consider the path $\mathbf{r}(\theta)=(r\cos\theta, r\sin\theta, h)$—that is, a circle of radius r at height h above the (x, y) plane. For this path, the Frenet directed frame specified by Equation (13) is

$$\mathbf{o} = \frac{(r\cos\theta, r\sin\theta, h)}{\sqrt{r^2+h^2}}$$
$$\mathbf{u} = (-\sin\theta, \cos\theta, 0)$$
$$\mathbf{v} = \frac{(-h\cos\theta, -h\sin\theta, r)}{\sqrt{r^2+h^2}}$$

Note that $\mathbf{u}$ coincides with the unit tangent $\mathbf{t}$ to the path. The polar distance, curvature, and torsion functions are all constant, namely

$$\rho = \sqrt{r^2+h^2} \qquad \lambda = \frac{r}{r^2+h^2} \qquad \upsilon = \frac{h}{r^2+h^2}$$

Since the parametric speed has the constant value $\sigma = r$, the angular speed of the Frenet directed frame is $|\mathbf{e}| = \rho\sqrt{\lambda^2+\upsilon^2}/\sigma = 1/r$, and for the RMDF we have $|\boldsymbol{\omega}| = \rho\lambda/\sigma = 1/\sqrt{r^2+h^2}$. Hence, the angular speeds coincide when $h = 0$, but for $h \gg r$ the angular speed of the RMDF is significantly lower. With $\psi_0 = 0$, the angle function (22) specifying the orientation of the RMDF relative to the Frenet direct frame is simply

$$\psi(\theta) = -\frac{\theta}{\sqrt{1+(r/h)^2}}$$

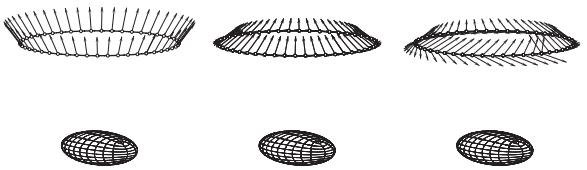

Figure 2. Left: variation of the polar vector $\mathbf{o}$ *around the path of Example 1. Center: variation of the Frenet directed frame vectors* $\mathbf{u}$ *and* $\mathbf{v}$ *(the* $\mathbf{u}$ *vectors are difficult to discern here, since they coincide with the curve tangent* $\mathbf{t}$*). Right: variation of the RMDF frame vectors* $\mathbf{p}$ *and* $\mathbf{q}$*—note that the RMDF does not, in general, exhibit a periodic variation along a smooth closed path.*

For a complete traversal of the path, the RMDF experiences a total rotation of $-2\pi/\sqrt{1+(r/h)^2}$ (always less than a full revolution) relative to the Frenet directed frame. Since the latter is of period 2π in θ, we see that the RMDF is not, in general, continuous around a closed path. Figure 2 illustrates the variation of the polar vector $\mathbf{o}$ and the directed frame pairs $(\mathbf{u}, \mathbf{v})$ and $(\mathbf{p}, \mathbf{q})$ orthogonal to it, in the case $r = 6$ and $h = 8$, while Figure 3 illustrates views of the ellipsoid oriented in accordance with these frames.

Example 2. Consider the circular helix[††] $\mathbf{r}(\theta) = (r\cos\theta, r\sin\theta, k\theta)$. Setting $c = k/r$, the Frenet directed frame is

$$\mathbf{o} = \frac{(\cos\theta, \sin\theta, c\theta)}{\sqrt{1+c^2\theta^2}}$$
$$\mathbf{u} = \frac{(-c^2\theta(\cos\theta+\theta\sin\theta) - \sin\theta,\ c^2\theta(\theta\cos\theta-\sin\theta)+\cos\theta,\ c)}{\sqrt{1+c^2\theta^2}\sqrt{1+c^2+c^2\theta^2}}$$
$$\mathbf{v} = \frac{(c(\sin\theta-\theta\cos\theta),\ -c(\cos\theta+\theta\sin\theta),\ 1)}{\sqrt{1+c^2+c^2\theta^2}}$$

while the polar distance and polar curvature and torsion are given by

$$\rho = r\sqrt{1+c^2\theta^2}$$
$$\lambda = \frac{\sqrt{1+c^2+c^2\theta^2}}{r(1+c^2\theta^2)^{3/2}}$$
$$\upsilon = \frac{c\theta}{r(1+c^2+c^2\theta^2)}$$

[††]This curve is not a *polar* helix in the sense of Remark 1, but the circle in Example 1 is—since it has constant polar curvature λ and polar torsion υ.

DOI: 10.1002/cav

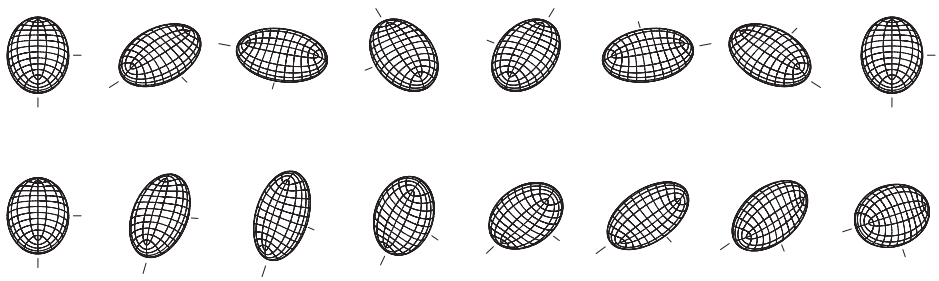

Figure 3. Comparison of ellipsoid views as the camera follows the path of Example 1, using the Frenet directed frame (upper) and rotation-minimizing directed frame (lower) to orient the camera image plane about its optical axis.

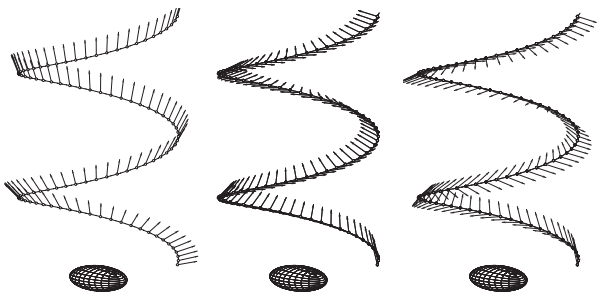

Figure 4. Left: the polar vector $\mathbf{o}$ *along the circular helix path of Example 2. Center: the Frenet directed frame vectors* $\mathbf{u}$ *and* $\mathbf{v}$ *spanning the image plane along this path. Right: the corresponding RMDF frame vectors* $\mathbf{p}$ *and* $\mathbf{q}$.

The orientation of the RMDF relative to the Frenet directed frame, given by Equation (22) with $\psi_0 = 0$, reduces to

$$\psi = \tan^{-1}\frac{\sqrt{1+c^2\theta^2}}{c} - \tan^{-1}\frac{1}{c} - \frac{\sqrt{1+c^2\theta^2}-1}{c}$$

Figure 4 illustrates the variation of the polar vector $\mathbf{o}$ along $\mathbf{r}(\theta)$, together with the Frenet vectors ($\mathbf{u}$, $\mathbf{v}$) and rotation-minimizing vectors ($\mathbf{p}$, $\mathbf{q}$) in the image plane, for the case $r = 8$, $k = 2$. Figure 5 shows a sampling of views of the ellipsoid, when the camera image plane is oriented by these vector pairs.

The polar curvature and torsion for this path are shown in Figure 6. Note that λ and υ both decrease with θ, decaying like θ^{-1} and θ^{-2} respectively for large θ. Thus, the difference between the Frenet directed frame and the rotation-minimizing frame becomes more pronounced with increasing θ.

Returning to the path in Figure 1 (a quintic Bézier curve), Figure 7 gives a comparison of the Frenet vectors ($\mathbf{u}$, $\mathbf{v}$) and rotation-minimizing vectors ($\mathbf{p}$, $\mathbf{q}$) spanning the image plane, while Figure 8 shows a sampling of views of the ellipsoid, oriented by these vectors. Figure 9 illustrates the variation of the polar curvature λ and polar torsion υ along this curve. Also shown are the angular speeds of the Frenet directed frame and the rotation-minimizing directed frame—$\rho\sqrt{\lambda^2+\upsilon^2}/\sigma$ and $\rho\lambda/\sigma$, respectively.

Pythagorean Curves

For the RMAF, the integrand in Equation (10) can be made rational[3] by choosing $\mathbf{r}(\xi)$ to be a spatial PH curve. A similar resolution is possible for the RMDF, but the coordinate components of the *curve* $\mathbf{r}(\xi) = (x(\xi), y(\xi), z(\xi))$—rather than its *hodograph* $\mathbf{r}'(\xi) = (x'(\xi), y'(\xi), z'(\xi))$—must be elements of a Pythagorean

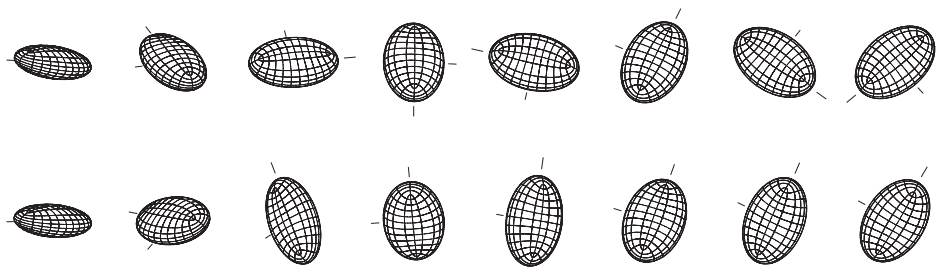

Figure 5. Comparison of ellipsoid views as the camera follows the path of Example 2, using the Frenet directed frame (upper) and rotation-minimizing directed frame (lower) to orient the camera image plane about its optical axis.

DOI: 10.1002/cav

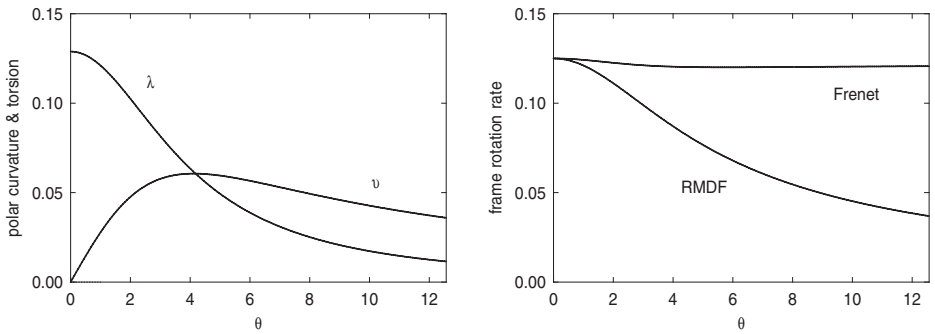

Figure 6. Left: variation of polar curvature λ and polar torsion υ along the path shown in Figure 4. Right: rotation rates $\rho\sqrt{\lambda^2+\upsilon^2}/\sigma$ and $\rho\lambda/\sigma$ for the Frenet directed frame and rotation-minimizing directed frame on this path.

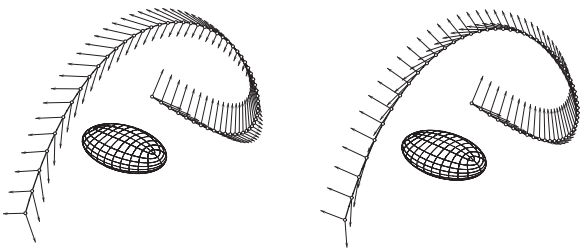

Figure 7. Comparison of the rotation-minimizing directed frame (left) with the Frenet directed frame (right) along the path shown in Figure 1. The two frames are identical at the initial curve point just above the ellipsoid target.

quartuple, that is, we must have

$$x^2(\xi) + y^2(\xi) + z^2(\xi) \equiv \rho^2(\xi)$$

for some polynomial $\rho(\xi)$. This condition characterizes a *Pythagorean curve*—or P curve—rather than a PH curve. The computation of exact RMDFs thus motivates a study of the properties and construction of P curves.

Many of the ideas and methods used in the study of PH curves carry over to the investigation of P curves (see Reference [23] for a detailed treatment of the theory of PH curves). In particular, the *quaternion formulation*[19,24,25] of spatial PH curves offers a convenient model for the construction of P curves.

A spatial P curve $\mathbf{r}(\xi)$ is characterized by the fact that its polar distance ρ from the origin is a polynomial in the curve parameter ξ. Since this is equivalent to the requirement that its anti-hodograph is a PH curve, the P curve can be expressed as a quaternion product[24] of the form

$$\mathbf{r}(\xi) = \mathcal{A}(\xi)\ \mathbf{i}\ \mathcal{A}^*(\xi) \qquad (23)$$

$\mathcal{A}(\xi) = u(\xi) + v(\xi)\mathbf{i} + p(\xi)\mathbf{j} + q(\xi)\mathbf{k}$ being a quaternion polynomial of degree m for a Pythagorean curve of degree $n = 2m$. We see that, whereas regular PH curves are of *odd* degree, polar-regular P curves are[‡‡] of *even* degree.

To solve practical design problems using P curves, intuitive methods for their construction are required. These are typically based on interpolation of discrete point and tangent data. We briefly describe two methods here. The first is based on classical Hermite interpolation of end-points and derivatives: $\mathbf{r}(0) = \mathbf{p}_i$, $\mathbf{r}'(0) = \mathbf{d}_i$, and $\mathbf{r}(1) = \mathbf{p}_f$, $\mathbf{r}'(1) = \mathbf{d}_f$. This employs P curves of degree six, and requires selection of three residual (scalar) parameters. In the second method, interpolation of end-derivatives is relaxed, and instead a middle interpolation point is introduced, $\mathbf{r}(\frac{1}{2}) = \mathbf{p}_m$. In this case, P curves of degree 4 can be defined, with two residual (scalar) degrees of freedom.

We present just basic outlines of these two methods below—in particular, we do not address the problem of optimal choices for the free parameters, since it is non-trivial and beyond our present scope. We use the Bézier form (17) for a P curve with control points $\mathbf{p}_0, \ldots, \mathbf{p}_n$ and assume the reader is familiar with the quaternion representation[19,25–27] of PH curves.

C^1 Hermite Interpolation by P Curves of Degree 6

To define a P curve of degree 6, we substitute a cubic quaternion polynomial

$$\mathcal{A}(\xi) = \mathcal{A}_0(1-\xi)^3 + \mathcal{A}_1 3(1-\xi)^2\xi + \mathcal{A}_2 3(1-\xi)\xi^2 + \mathcal{A}_3\xi^3$$

[‡‡]P curves of odd degree may be defined by multiplying the right-hand side of Equation (23) by a scalar odd-degree polynomial $f(\xi)$, but in general these curves are not polar-regular since $\rho(\xi) = |f(\xi)|\,|\mathcal{A}(\xi)|^2$ will vanish at the real roots, if any, of $f(\xi)$.

DOI: 10.1002/cav

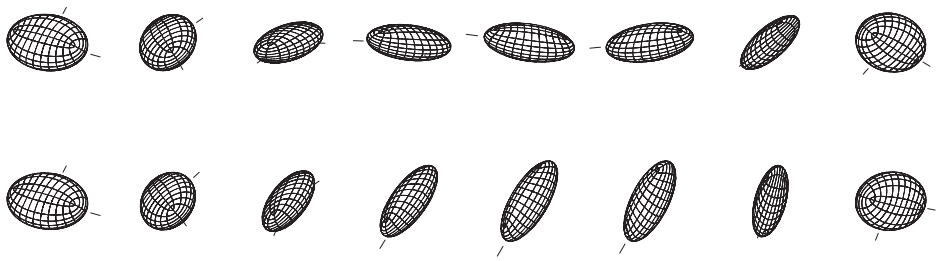

Figure 8. Comparison of ellipsoid views as the camera follows the path shown in Figure 1, using the Frenet directed frame (upper) and rotation-minimizing directed frame (lower) to orient the camera image plane about its optical axis.

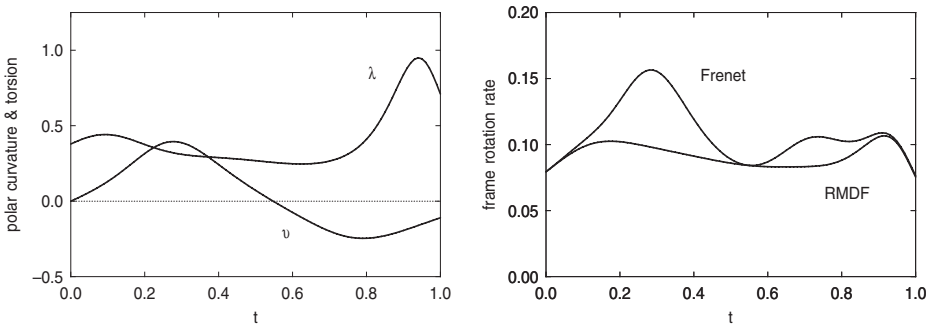

Figure 9. Left: variation of polar curvature λ and polar torsion υ along the path shown in Figure 1. Right: rotation rates $\rho\sqrt{\lambda^2+\upsilon^2}/\sigma$ and $\rho\lambda/\sigma$ for the Frenet directed frame and rotation-minimizing directed frame on this path.

into expression (23). The control points $\mathbf{p}_i = x_i\mathbf{i} + y_i\mathbf{j} + z_i\mathbf{k}$ of the Bézier form (17) are then given by

$$\begin{aligned}
\mathbf{p}_0 &= \mathcal{A}_0\mathbf{i}\mathcal{A}_0^* \\
\mathbf{p}_1 &= \tfrac{1}{2}(\mathcal{A}_0\mathbf{i}\mathcal{A}_1^* + \mathcal{A}_1\mathbf{i}\mathcal{A}_0^*) \\
\mathbf{p}_2 &= \tfrac{1}{5}(\mathcal{A}_0\mathbf{i}\mathcal{A}_2^* + 3\mathcal{A}_1\mathbf{i}\mathcal{A}_1^* + \mathcal{A}_2\mathbf{i}\mathcal{A}_0^*) \\
\mathbf{p}_3 &= \tfrac{1}{20}(\mathcal{A}_0\mathbf{i}\mathcal{A}_3^* + 9\mathcal{A}_1\mathbf{i}\mathcal{A}_2^* + 9\mathcal{A}_2\mathbf{i}\mathcal{A}_1^* + \mathcal{A}_3\mathbf{i}\mathcal{A}_0^*) \\
\mathbf{p}_4 &= \tfrac{1}{5}(\mathcal{A}_1\mathbf{i}\mathcal{A}_3^* + 3\mathcal{A}_2\mathbf{i}\mathcal{A}_2^* + \mathcal{A}_3\mathbf{i}\mathcal{A}_1^*) \\
\mathbf{p}_5 &= \tfrac{1}{2}(\mathcal{A}_2\mathbf{i}\mathcal{A}_3^* + \mathcal{A}_3\mathbf{i}\mathcal{A}_2^*) \\
\mathbf{p}_6 &= \mathcal{A}_3\mathbf{i}\mathcal{A}_3^*
\end{aligned}$$

Interpolation of the two end points yields the equations

$$\mathcal{A}_0\mathbf{i}\mathcal{A}_0^* = \mathbf{p}_i \quad \text{and} \quad \mathcal{A}_3\mathbf{i}\mathcal{A}_3^* = \mathbf{p}_f \tag{24}$$

for $\mathcal{A}_0$ and $\mathcal{A}_3$, while interpolation of the end derivatives gives the equations

$$\tfrac{1}{2}\left(\mathcal{A}_0\mathbf{i}\mathcal{A}_1^* + \mathcal{A}_1\mathbf{i}\mathcal{A}_0^*\right) = \mathbf{g}_i \quad \text{and} \quad \tfrac{1}{2}\left(\mathcal{A}_2\mathbf{i}\mathcal{A}_3^* + \mathcal{A}_3\mathbf{i}\mathcal{A}_2^*\right) = \mathbf{g}_f \tag{25}$$

for $\mathcal{A}_1$ and $\mathcal{A}_2$, where we set

$$\mathbf{g}_i = \mathbf{p}_i + \tfrac{1}{6}\mathbf{d}_i \quad \text{and} \quad \mathbf{g}_f = \mathbf{p}_f - \tfrac{1}{6}\mathbf{d}_f$$

The Equations (24) are of the well-known form $\mathcal{A}\mathbf{i}\mathcal{A}^* = \mathbf{d}$, where $\mathbf{d}$ is any non-zero vector not aligned with $-\mathbf{i}$, and can be solved directly[26] to obtain

$$\mathcal{A}_0 = \sqrt{|\mathbf{p}_i|}\mathbf{n}_i \exp(\phi_i\mathbf{i}) \quad \text{and} \quad \mathcal{A}_3 = \sqrt{|\mathbf{p}_f|}\mathbf{n}_f \exp(\phi_f\mathbf{i})$$

where ϕ_i and ϕ_f are free angular variables, and we define

$$\boldsymbol{\delta}_i = \frac{\mathbf{p}_i}{|\mathbf{p}_i|} \quad \mathbf{n}_i = \frac{\boldsymbol{\delta}_i + \mathbf{i}}{|\boldsymbol{\delta}_i + \mathbf{i}|} \tag{26}$$

and

$$\boldsymbol{\delta}_f = \frac{\mathbf{p}_f}{|\mathbf{p}_f|} \quad \mathbf{n}_f = \frac{\boldsymbol{\delta}_f + \mathbf{i}}{|\boldsymbol{\delta}_f + \mathbf{i}|} \tag{27}$$

On the other hand, the Equations (25) are of the form cited in Lemma 2.5 of Reference [27], and can be solved directly to obtain

$$\mathcal{A}_1 = -\frac{(\mu_i + \mathbf{g}_i)\mathcal{A}_0\mathbf{i}}{|\mathcal{A}_0|^2} \quad \text{and} \quad \mathcal{A}_2 = -\frac{(\mu_f + \mathbf{g}_f)\mathcal{A}_3\mathbf{i}}{|\mathcal{A}_3|^2}$$

DOI: 10.1002/cav

where μ_i and μ_f are free real parameters. As shown in the PH curve context,[25] the P curve (23) depends only on the *difference* $\Delta\phi = \phi_f - \phi_i$. Hence, solutions to the problem of Hermite interpolation by P curves of degree 6 depend on three real parameters—$\Delta\phi$, μ_i, and μ_f.

C^0 Three-point Interpolation by P Curves of Degree 4

Given points $\mathbf{p}_i$, $\mathbf{p}_m$, $\mathbf{p}_f$, we seek a P curve interpolant $\mathbf{r}(\xi)$ satisfying $\mathbf{r}(0) = \mathbf{p}_i$, $\mathbf{r}(\frac{1}{2}) = \mathbf{p}_m$, $\mathbf{r}(1) = \mathbf{p}_f$. Substituting the quadratic quaternion polynomial

$$\mathcal{A}(\xi) = \mathcal{A}_0(1-\xi)^2 + \mathcal{A}_1 2(1-\xi)\xi + \mathcal{A}_2\xi^2$$

into Equation (23) gives a quartic P curve, specified in the form (17) by control points

$$\begin{aligned}
\mathbf{p}_0 &= \mathcal{A}_0\mathbf{i}\mathcal{A}_0^* \\
\mathbf{p}_1 &= \tfrac{1}{2}(\mathcal{A}_0\mathbf{i}\mathcal{A}_1^* + \mathcal{A}_1\mathbf{i}\mathcal{A}_0^*) \\
\mathbf{p}_2 &= \tfrac{1}{6}(\mathcal{A}_0\mathbf{i}\mathcal{A}_2^* + 4\mathcal{A}_1\mathbf{i}\mathcal{A}_1^* + \mathcal{A}_2\mathbf{i}\mathcal{A}_0^*) \\
\mathbf{p}_3 &= \tfrac{1}{2}(\mathcal{A}_1\mathbf{i}\mathcal{A}_2^* + \mathcal{A}_2\mathbf{i}\mathcal{A}_1^*) \\
\mathbf{p}_4 &= \mathcal{A}_2\mathbf{i}\mathcal{A}_2^*
\end{aligned}$$

As in the previous case, interpolation of end points yields the equations

$$\mathcal{A}_0\mathbf{i}\mathcal{A}_0^* = \mathbf{p}_i \quad \text{and} \quad \mathcal{A}_2\mathbf{i}\mathcal{A}_2^* = \mathbf{p}_f$$

with solutions

$$\mathcal{A}_0 = \sqrt{|\mathbf{p}_i|}\mathbf{n}_i \exp(\phi_i\mathbf{i}) \quad \text{and} \quad \mathcal{A}_2 = \sqrt{|\mathbf{p}_f|}\mathbf{n}_f \exp(\phi_f\mathbf{i})$$

where ϕ_i, ϕ_f are free angular variables, and $\mathbf{n}_i$, $\mathbf{n}_f$ are as in Equations (26) and (27). Now since

$$\mathbf{r}\left(\tfrac{1}{2}\right) = \tfrac{1}{16}(\mathcal{A}_0 + 2\mathcal{A}_1 + \mathcal{A}_2)\mathbf{i}(\mathcal{A}_0^* + 2\mathcal{A}_1^* + \mathcal{A}_2^*)$$

the interpolation condition $\mathbf{r}(\frac{1}{2}) = \mathbf{p}_m$ yields

$$\mathcal{B}\mathbf{i}\mathcal{B}^* = \mathbf{d}$$

where we set $\mathcal{B} = \mathcal{A}_0 + 2\mathcal{A}_1 + \mathcal{A}_2$ and $\mathbf{d} = 16\mathbf{p}_m$. Hence, we have

$$\mathcal{B} = \sqrt{|\mathbf{d}|}\mathbf{n}_m \exp(\phi_m\mathbf{i})$$

where ϕ_m is another free angular variable, and we define

$$\boldsymbol{\delta}_m = \frac{\mathbf{d}}{|\mathbf{d}|} \quad \mathbf{n}_m = \frac{\boldsymbol{\delta}_m + \mathbf{i}}{|\boldsymbol{\delta}_m + \mathbf{i}|}$$

Since the quartic P curve (23) depends only on the differences of ϕ_i, ϕ_m, ϕ_f, the three-point interpolants depend on just two free parameters.

Conclusion

A *directed* orthonormal frame on a space curve is characterized by the fact that one frame vector corresponds to the unit polar vector from the origin to each curve point, while the other two frame vectors span the "image plane" orthogonal to this polar vector. A special instance, the Frenet directed frame, is identified by analogy with the *adapted* orthonormal frames on space curves, for which one vector corresponds to the curve tangent. Specifically, the theory of the Frenet directed frame coincides with that of the Frenet adapted frame, applied to the *anti-hodograph* of the given curve. This analogy motivates us to introduce the *polar curvature* and *polar torsion* of space curves.

RMDFs may offer a useful camera orientation control strategy, in applications such as the navigation of virtual environments, interactive computer games, and endoscopic surgery imaging, as an alternative to the usual maintenance of vertical orientation. The RMDF was shown to be related to the Frenet directed frame, through an angular displacement function specified by the integral of the polar torsion. For the special family of *Pythagorean* (P) *curves*, this integral admits a closed-form evaluation by the partial fraction expansion of a rational function. Much of the established theory for the *PH curves*[23] can be adapted to the construction and analysis of P curves. Similarly, the theory of *double PH curves*[20,22,28] can be modified to define *double P curves*, having *rational* Frenet directed frames and polar curvature and torsion functions.

References

1. Klok F. Two moving coordinate frames for sweeping along a 3D trajectory. *Computer Aided Geometric Design* 1986; **3**: 217–229.
2. Guggenheimer H. Computing frames along a trajectory. *Computer Aided Geometric Design* 1989; **6**: 77–78.

DOI: 10.1002/cav

3. Farouki RT. Exact rotation-minimizing frames for spatial Pythagorean-hodograph curves. *Graphical Models* 2002; **64**: 382–395.
4. Farouki RT, Han CY. Rational approximation schemes for rotation-minimizing frames on Pythagorean-hodograph curves. *Computer Aided Geometric Design* 2003; **20**: 435–454.
5. Jüttler B. Generating rational frames of space curves via Hermite interpolation with Pythagorean hodograph cubic splines. In *Geometric Modeling and Processing'98*, Chi DP, Choi HI, Kim MS, Martin R (eds). Bookplus Press: Pohang, Korea 1998; 83–106.
6. Jüttler B, Mäurer C. Cubic Pythagorean hodograph spline curves and applications to sweep surface modelling. *Computer Aided Design* 1999; **31**: 73–83.
7. Jüttler B, Mäurer C. Rational approximation of rotation minimizing frames using Pythagorean-hodograph cubics. *Journal for Geometry and Graphics* 1999; **3**: 141–159.
8. Wang W, Joe B. Robust computation of the rotation minimizing frame for sweep surface modelling. *Computer Aided Design* 1997; **29**: 379–391.
9. Christie M, Machap R, Normad J-M, Oliver P, Pickering J. Virtual camera planning: a survey. In *Proceedings of Smart Graphics 2005*, Lecture Notes in Computer Science 3638, Butz A, Fisher B, Kruger A, Olivier P (eds). Springer: Berlin, 2005; 40–52.
10. Nieuwenhuisen D, Overmars MH. Motion planning for camera movements. In *Proceedings, IEEE International Conference on Robotics & Automation*, New Orleans, LA, April 2004 ; 3870–3876.
11. Cao CGL. Guiding navigation in colonoscopy. *Surgical Endoscopy* 2007; **21**: 408–484.
12. Colt HG, Crawford SW, Galbraith O, III. Virtual reality bronchoscopy simulation: a revolution in procedural training. *Chest* 2001; **120**: 1333–1339.
13. Holden JG, Flach JM, Donchin Y. Perceptual-motor coordination in an endoscopic surgery simulation. *Surgical Endoscopy* 1999; **13**: 127–132.
14. Solomon SB, White P, Jr., Wiener CM, Orens JB, Wang KP. Three-dimensional CT-guided bronchoscopy with a real-time electromagnetic position sensor: a comparison of two image registration methods. *Chest* 2000; **118**: 1783–1787.
15. Mattsson-Boze D, Chatenever D. Image orientation for endoscopic video displays, United States Patent 6097423, http://www.freepatentsonline.com/6097423.html, 2000.
16. Schara JN, Hoeg HD, Hale EL. Gravity referenced endoscopic image orientation, United States Patent 7134992, http://www.freepatentsonline.com/7134992.html, 2006.
17. Kreyszig E. *Differential Geometry*. University of Toronto Press: Toronto, 1959.
18. Bishop RL. There is more than one way to frame a curve. *American Mathematical Monthly* 1975; **82**: 246–251.
19. Farouki RT, al-Kandari M, Sakkalis T. Structural invariance of spatial Pythagorean hodographs. *Computer Aided Geometric Design* 2002; **19**: 395–407.
20. Beltran JV, Monterde J. A characterization of quintic helices. *Journal of Computational and Applied Mathematics* 2007; **206**: 116–121.
21. Farouki RT, Han CY, Manni C, Sestini A. Characterization and construction of helical polynomial space curves. *Journal of Computational and Applied Mathematics* 2004; **162**: 365–392.
22. Monterde J. A characterization of helical polynomial curves of any degree. *Advances in Computational Mathematics*, 2008, to appear.
23. Farouki RT. *Pythagorean-hodograph Curves: Algebra and Geometry Inseparable*. Springer: Berlin, 2008.
24. Choi HI, Lee DS, Moon HP. Clifford algebra, spin representation, and rational parameterization of curves and surfaces. *Advances in Computational Mathematics* 2002; **17**: 5–48.
25. Farouki RT, al-Kandari M, Sakkalis T. Hermite interpolation by rotation-invariant spatial Pythagorean-hodograph curves. *Advances in Computational Mathematics* 2002; **17**: 369–383.
26. Farouki RT, Giannelli C, Manni C, Sestini A. Identification of spatial PH quintic Hermite interpolants with near-optimal shape measures. *Computer Aided Geometric Design* 2008; **25**: 274–297.
27. Sir Z, Jüttler B. C^2 Hermite interpolation by Pythagorean hodograph space curves. *Mathematics of Computation* 2007; **76**: 1373–1391.
28. Farouki RT, Giannelli C, Sestini A. Helical polynomial curves and double Pythagorean hodographs I. Quaternion and Hopf map representations & II. Enumeration of low-degree curves. *Journal of Symbolic Computation*, 2008, to appear.

Authors' biographies:

Rida T. Farouki is Professor of Mechanical and Aeronautical Engineering at the University of California, Davis. He received the B.A. degree in Engineering Science from Oxford University and the Ph.D. in Astronomy and Space Sciences from Cornell University, and worked for ten years in the research divisions of GE and IBM prior to returning to academic life. He is author or co-author of more than 100 research publications concerned with geometrical algorithms, computer-aided design and manufacturing, numerical analysis, stellar dynamics, plasma physics, and geometric optics. He is also author of the monograph Pythagorean-Hodograph Curves: Algebra and Geometry Inseparable, published by Springer in 2008.

DOI: 10.1002/cav

Carlotta Giannelli is a Ph.D. student in Computer Science and Applications in the Department of Systems and Computer Science at the University of Florence, Italy. She received the Laurea in Computer Science from the University of Florence in 2006. Her primary research interests focus on numerical and scientific computing related to computer aided geometric design.

DOI: 10.1002/cav